Comparison of transmissive and reflective SLMs for the emulation of discontinuous wavefronts

Evan O'Rourke, Deborah Malone, Nicholas Devaney

AO4ELT7 - June 2023 - Avignon

Comparison of transmissive and reflective SLMs for the emulation of discontinuous wavefronts

Evan O'Rourke[a], Deborah Malone[a], and Nicholas Devaney[a]

[a]Applied Optics, University of Galway, Ireland

ABSTRACT

It has been known for some time that the Low Wind Effect (LWE) has the potential to severely limit the quality of images obtained using adaptive optics on ELTs. This effect, and ways to measure the resulting piston between 'petals' of the telescope pupil is an active area of research, relying mostly on numerical simulations, and also laboratory experiments using reflective spatial light modulators (SLMs). In the work presented here, we investigate using a transmissive SLM to simulate the petalling effect. This type of SLM is very easy to incorporate into an experimental setup, and has a lower cost than reflective SLMs. The fact that transmissive SLMs are thicker (for the same simulated wavefront error) and therefore slower is not so important for this application. We describe a laboratory setup to demonstrate petalling, including a simple interferometric technique to measure the piston errors. The ability of transmissive and reflective SLMs to generate discontinuous wavefronts is examined and compared.

Keywords: Spatial light modulators, discontinuous wavefronts, reflective SLM, transmissive SLM, wavefront petalling, petal

1. INTRODUCTION

The Low Wind Effect (LWE) was first described by Sauvage et al. in 2015 [4]. It was discovered on the Spectro Polarimetric High contrast Exoplanet REsearch (SPHERE) instrument installed on the Very Large Telescope (VLT). During the first commissioning of SPHERE, it was discovered that the first of the circular Airy rings of a single star splits into several pieces when the wind speed at the telescope was below 3 m/s [7]. It was discovered that the secondary mirror structure (known as the spider) was the cause of the effect. Radiative transfer between the spider arm and the surrounding air caused differences in refractive indices on either side, producing an optical path difference. This presents itself in the wavefront as a strong discontinuity across the spider, which is difficult to measure with conventional wavefront sensors (WFS) such as the Shack-Hartmann [5].

While the LWE can be reduced greatly by the application of a low thermal emissivity coating, it cannot be eliminated entirely. Milli et al. note that the application of NanoBlack^{TM} reduced the appearance of the effect from below wind speeds of 3 m/s to only below 1 m/s, a change from 19.4% of the observation time down

Further author information: (Send correspondence to D.M)
E.O.R: E-mail: e.orourke4@nuigalway.ie
D.M: E-mail: deborah.malone@universityofgalway.ie
N.D: E-mail: nicholas.devaney@universityofgalway.ie

to 3.5% [3]. As the effect cannot be entirely eliminated at this time, it is important to investigate methods of further reducing the effect. This is especially important in the case of future telescopes, such as the European Extremely Large Telescope (E-ELT), which is also expected to be affected by the LWE. To do this, it is important to accurately simulate the petalling effect the telescope might experience.

In this paper will we test a commercially available low-cost transmissive SLM's ability to produce petalling, and use techniques employed in Sparse Aperture Wavefront Sensing (SAWFS) to recover the phase. Additionally, we will compare this SLM's ability to produce a discontinuous wavefront to a reflective SLM using the Peak Ratio Comparison (PRC) method.

2. METHODS

2.1 Sparse Aperture Wavefront Sensing (SAWFS)

The concept of applying Sparse Aperture Wavefront Sensing to petal sensing was introduced by Deo et al. in 2022 [1]. The method uses techniques from sparse aperture masking interferometry, which samples the pupil with an array of smaller holes. These holes use non-redundant baselines, i.e. no two baselines between the holes are the same length and orientation. At the focal plane, and interferogram is formed instead of a classical PSF. Each pair of holes on the pupil mask creates interference fringes, and the interferogram is a superposition of these. The number of sets of fringes, n_f is described by Equation 1, where N is the number of apertures in the mask.

$$n_f = \frac{N(N-1)}{2} \tag{1}$$

Taking the Two-dimensional Fourier transform of the interferogram then gives the autocorrelation of the electric field in the pupil plane. The complex argument from this resulting autocorrelation provides a way to measure the optical path differences (OPD) between all the holes by using Equation 2 on the resulting secondary spots in the Fourier domain.

$$\phi = \tan^{-1} \frac{Im(\text{peak})}{Re(\text{peak})} \tag{2}$$

In this paper, we study the use of SAWFS in combination with spatial light modulators to understand the concept, and compare laboratory results with simulations.

2.2 Peak Ratio Comparison (PRC)

In order to compare the ability of both SLMs to produce a discontinuity, we employ the method outlined by Schumacher, Devaney, and Montoya [6], which is a modification of the technique used at the W. M. Keck Observatory for phasing segmented primary mirrors. It uses a small circular aperture centred on the discontinuity. As the phase difference between the two sides increases, the point spread function (PSF) gradually splits into two peaks, with these peaks being equal when the phase difference is $\lambda/2$. The PSF then returns to a single peak when the phase difference is a multiple of λ. By comparing the ratio of the two peaks, it is possible to determine the phase difference between the two sides.

$$\text{Ratio} = \frac{\max(\text{Right Peak})}{\max(\text{Left Peak})} \tag{3}$$

2.3 Spatial Light Modulators (SLM)

This work will use two SLMs. The first one, used for the SAWFS experiments, is a transmissive nematic SLM manufactured by HOLOEYE Photonics AG. The second one, used as a comparison for generation of phase discontinuities, is a reflective nematic SLM manufactured by Boulder Non-linear Systems (BNS).

The reflective SLM (RSLM) is more difficult to incorporate into an established set-up, requiring either a very small angle of incidence, or a beam splitter which would reduce the overall throughput of the setup. The TSLM, is much cheaper than the reflective one, and can be more easily added to an optical system.

For both SLMs, the phase change is controlled via the rotation of liquid crystals (LCs). This is achieved via the application of voltages which are controlled by grey levels. For both SLMs, the grey levels range between 0 and 255. However, the LC types in each SLM differ. In the TSLM, the liquid crystals are of the twisted nematic type. This means that the liquid crystal molecules form a helix structure, where the angle of the molecular axis changes along the optical path. If the incident light has a polarisation parallel to the molecules at the entrance face, then the polarisation will follow the helical structure of the molecules and leave the cell with a polarisation perpendicular to the incident polarisation. As the voltage increases, the molecules become untwisted, and the rotation of the polarisation becomes less effective, until at some maximum voltage V_{max}, there is no rotation of the polarization. The characteristics of the twisted nematic LCs mean that one cannot operate the TSLM in a phase-only configuration. Instead, it can operate in a so-called phase-mostly mode, where there is still some weak amplitude modulation. The RSLM, on the other hand, has parallel-aligned LCs, which do not have this issue. Incident light which has its polarisation parallel to the LC molecules will have its polarisation unchanged, regardless of the applied voltage, and only the phase will be effected. The specifications of these SLMs are given in Table 1.

Table 1: Specifications of the transmissive and reflective SLMs compared in this article. Values given are taken from the manufacturer's manuals for the respective devices.

	TSLM	**RSLM**
Manufacturer	HOLOEYE Photonics AG	Boulder Non-linear Systems
Model	LC2012	P512-0532
Resolution	1024×768	512×512
Pixel Diameter	$36\,\mu$m	$15\,\mu$m
Phase Modulation	1.8π (@ 532 nm)	$\geq 2\pi$ (@ 532 nm)
LC Type	Twisted Nematic	Parallel-Aligned Nematic

2.4 Experimental Setup

Sparse Aperture Wavefront Sensing (SAWFS)

For this experiment, the OptiXplorer Education kit from HOLOEYE Photonics AG is used, which consists of a 532 nm laser with attached collimator, two polarisers, and the transmissive SLM. The experimental set-up is shown in Figure 1. The experiment uses a non-redundant mask consisting of 6 holes with unused holes blocked as needed to create a 2 and 4-hole mask. A microscope objective with a magnification of 20x and a numerical aperture of 0.50 is used to re-image the PSF onto a larger area on the detector.

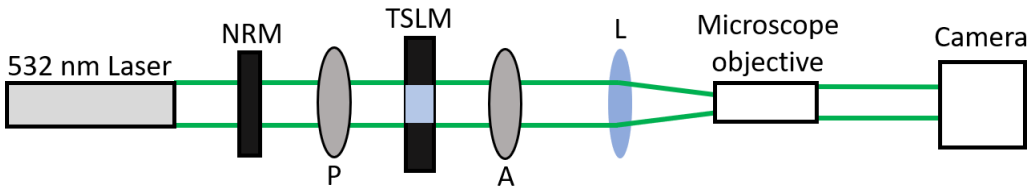

Figure 1: Set up for the SAWFS experiment. NRM = non-redundant mask, P = polariser, TSLM = Transmissive SLM, A = Analyser, L = lens. A microscope objective is used to increase the size of the PSF on the detector, magnification = 20x, numerical aperture 0.50.

Peak Ratio Comparison

The set-up from the SAWFS experiment is re-used here with the transmissive SLM, but with the microscope objective removed, and the focusing lens swapped out for one with a focal length of 150 mm. The non-redundant mask is re-used for this experiment, with every hole blocked except one. The mask is re-positioned so that the hole is centred on the phase discontinuity. For the reflective SLM, one polariser is removed, and a beam splitter is added to the optical path to allow the reflected light from the RSLM to be picked off at an angle and into the camera. The bench set-ups for the transmissive and reflective SLM are shown in Figures 3 and 4 respectively.

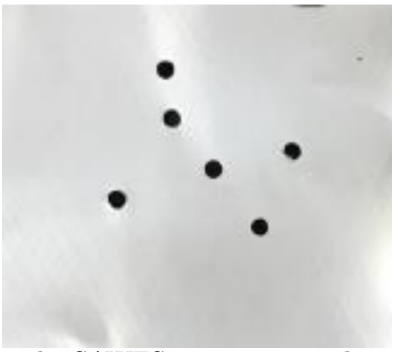

Figure 2: Non-redundant mask used for the SAWFS experiment. Thin sheet of aluminium with 1.5 mm holes. Unused holes were blocked as needed.

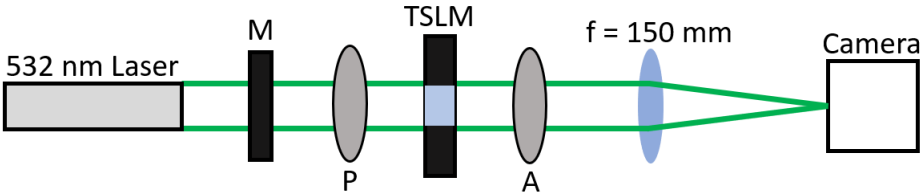

Figure 3: Set up for the transmissive SLM experiment. M = mask, P = polariser, TSLM = Transmissive SLM, A = Analyser.

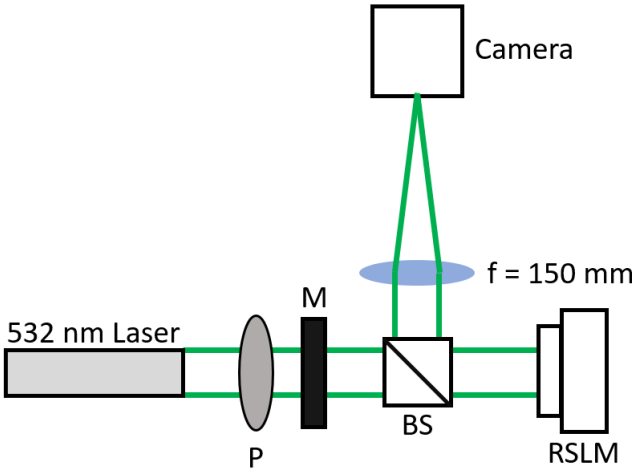

Figure 4: Set up for the reflective SLM experiment. P = polariser, M = mask, BS = Beam Splitter, RSLM = Reflective SLM

3. RESULTS

3.1 Sparse Aperture Wavefront Sensing

3.1.1 Numerical Simulation

The experiment is first simulated numerically. Figure 5 shows the simulated masks, corresponding point spread functions (PSFs), and pupil auto-correlations (obtained by Fourier Transforming the PSFs).

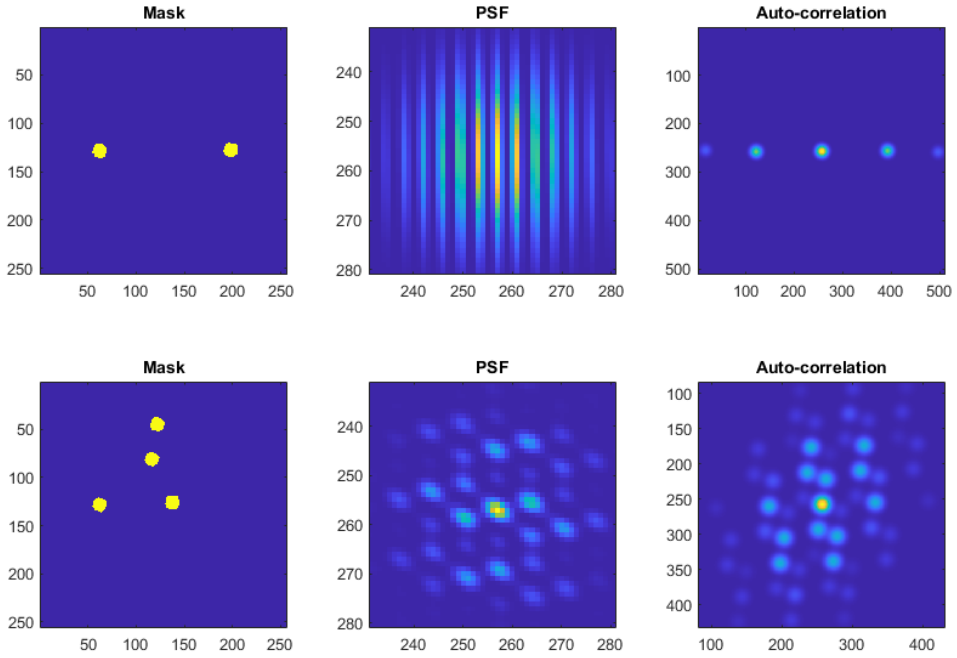

Figure 5: Examples of Interferograms and resulting Fourier transforms for 2 and 4 hole masks.

Theory suggests that by taking the value from one of these secondary spots and using Equation 2, the phase can be retrieved. We performed this calculation using a simulated two-hole mask. The Intensity of an interference pattern can be described as a superposition of $\cos^2$ functions, described by Equation 4.

$$I = 4I_0 \cos^2(\phi/2) \tag{4}$$

Ignoring the intensity, and only considering the phase, we can generate a PSF using the $\cos^2$ function, and shifting the phase ϕ by some small amount $\delta\phi$, given by Equation 5.

$$PSF = \cos^2\left(\frac{\phi + \delta\phi}{2}\right) \tag{5}$$

For this experiment, a PSF with a Gaussian intensity and noise is generated using the $\cos^2$ function, where $\delta\phi$ varies between 0 and 2π. In Figure 6 you can see the simulated PSF, the resulting auto-correlation, and the retrieved phase vs input phase when using Equation 2 on the right spot in the auto-correlation image.

The simulations show that the input phase shift ($\delta\phi$) is successfully retrieved using this method, even with added noise. However, this simple simulation does not account for any imperfections in an optical set-up, or effects due to external sources.

For multiple-hole masks, each spot would correspond to a pair of apertures from the non-redundant mask. Measuring all of these spots together gives a low-order interpretation of the relative phase off-sets between sections of the phase mask or segmented mirror, etc.

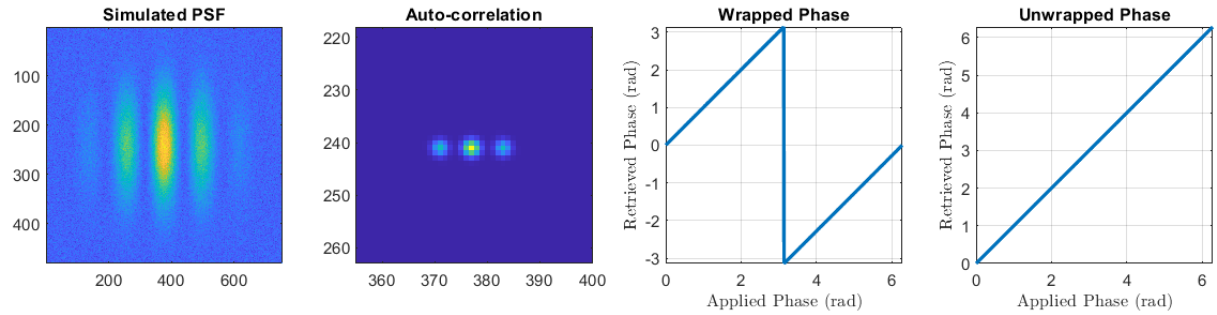

Figure 6: Numerically simulated PSF generated using Equation 5 multiplied by a Gaussian (to approximately simulate using finite sized holes) and added Gaussian-distributed noise. The right spot in the auto-correlation image is used along with Equation 2 to retrieve the phase, shown wrapped and unwrapped in the two graphs on the right.

3.1.2 Bench Results

In the lab, a set-up using 2-holes in the mask is used first. On the SLM, the array is split into two halves, with one being held at a fixed grey level of 0, and the other varying from 0 to 250 in steps of 10. The mask is positioned so that the two holes are on either side of the discontinuity. The resulting PSF is an interference pattern as expected, and getting the Fourier transform of this results in an auto-correlation image. By using Equation 2, the value of the phase difference between the pair of apertures corresponding to the spot can be retrieved, and is plotted against the difference in grey level between the two sides of the SLM.

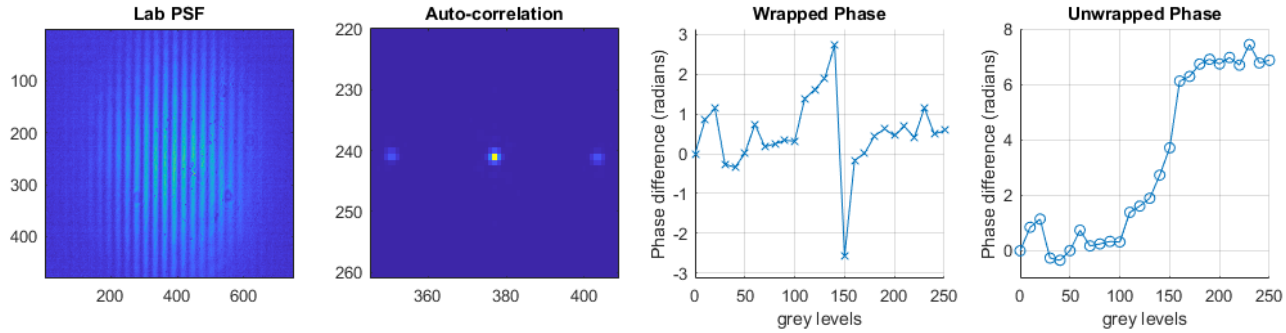

Figure 7: PSF and auto-correlation of the two-aperture mask as seen in the lab, along with the retrieved phase using the left spot.

The phase is measured from the left spot on the auto-correlation image in Figure 7. There is a discontinuity, which was expected, at a grey level of 150, suggesting that at this point the phase difference between the two sides of the SLM is π, or $\lambda/2$. The unwrapped phase has a linear region, with little response at low or high phase difference.

When using the 4-hole mask, the Phase shown in Figure 9 was used, however. In Figure 8, the phase changes between apertures corresponding to auto-correlation spots 4, 5, and 6, can be seen while 1, 2, and 3 do not change. With one aperture centred in the lower left corner which has the changing grey levels, and the other three in the other three quadrants, three pairs would show a changing phase difference, while the other three do not.

The unwrapped phase images from Figure 7 and 8 show that a phase change is retrievable using this method. The deviations from the expected linear response can be attributed to a non-optimal grey level to phase response for the transmissive SLM, which is close to, but not completely, linear.

3.2 Peak Ratio Comparison

Peak Ratio comparison was used to compare the ability of a transmissive SLM and a reflective one to generate a piston step. One side of the SLM is held at 0 while the other varies between 0 and 255 in steps of 5 with a single

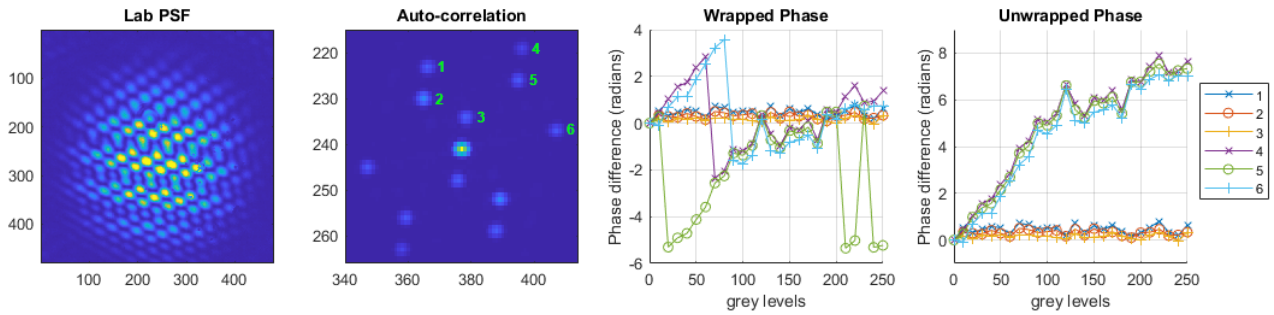

Figure 8: PSF, auto-correlation and resulting phase retrieved from the spots from the auto-correlation. 1-6 on the auto-correlation image correspond to 1-6 on the phase graphs, the legend on the right applies to both phase graphs, wrapped and unwrapped.

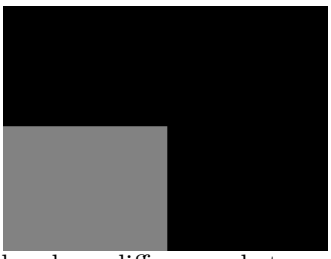

Figure 9: Phase screen used to generate the phase differences between sections of the wavefront. The lower left corner (shown in grey) had its grey levels vary between 0 and 250, while the rest of the phase screen was set to a grey level of 0.

hole centred on the discontinuity. The results are shown in Figure 10. Line profiles of the PSF's can be seen in Figure 11.

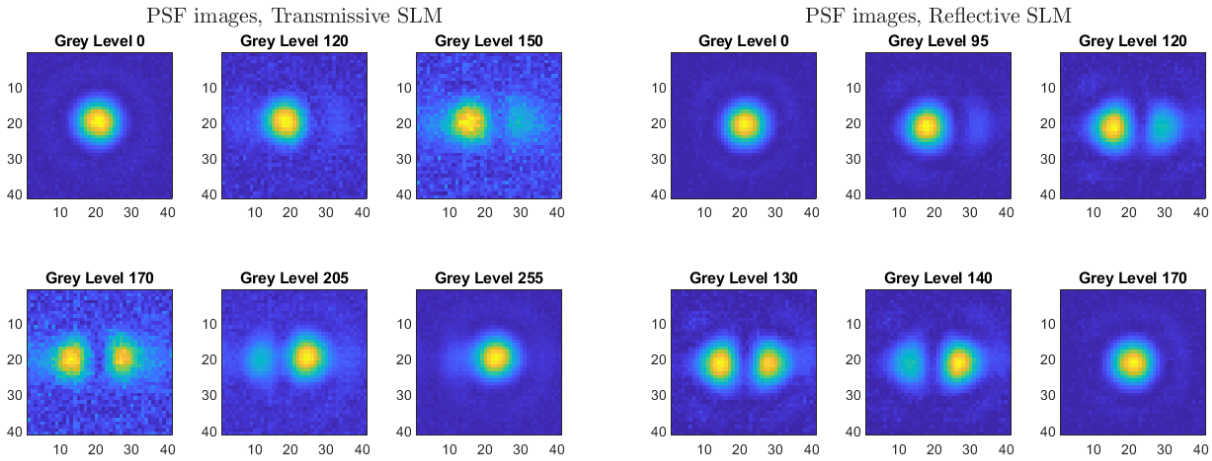

(a) (b)

Figure 10: PSFs taken of SLM with sides of different grey levels. Here you can see the grey levels at which the phase difference between the two sides were equal to π for each SLM (170 for TSLM (a), 130 for RSLM(b)). Also apparent here is that the RSLM achieves a full wave of phase change over only 170 grey levels, while the TSLM does not achieve a full wave.

From Figures 10 and 11, it is clear that the reflective SLM not only produces the most amount of phase change, but does so with a much higher signal-to-noise ratio. The properties of the twisted nematic liquid crystals on the transmissive SLM also produces an amplitude modulation, which reduces the throughput when the difference in

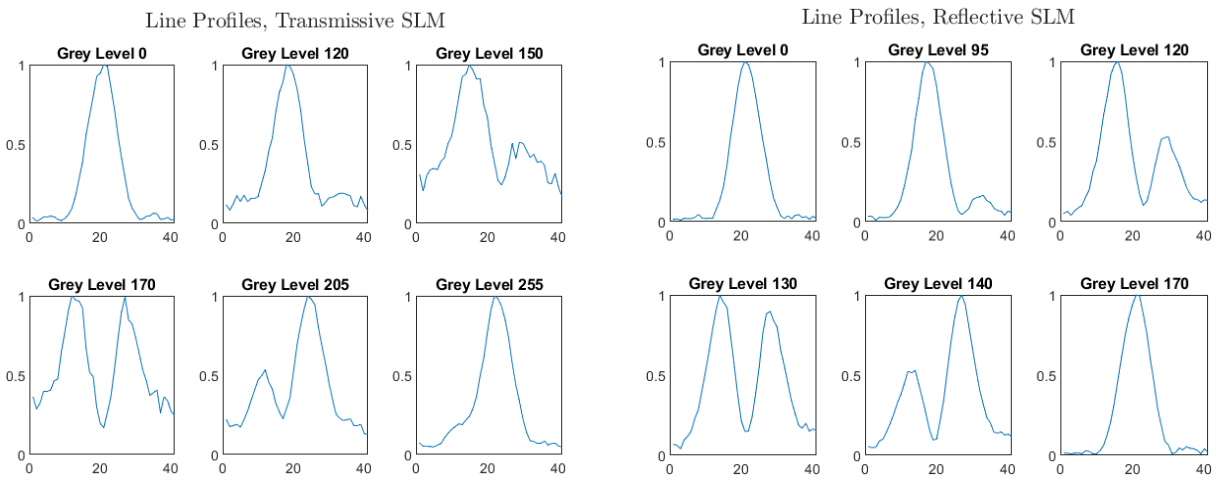

(a) (b)

Figure 11: Normalised x projection of PSF's from Figure 10b for the TSLM (a) and the RSLM (b).

phase between the two sides is $\approx \pi$. This is better visualised in a non-normalised diagram, which can be seen in Figure 12 where the line profiles are plotted together to produce a "Slice Diagram".

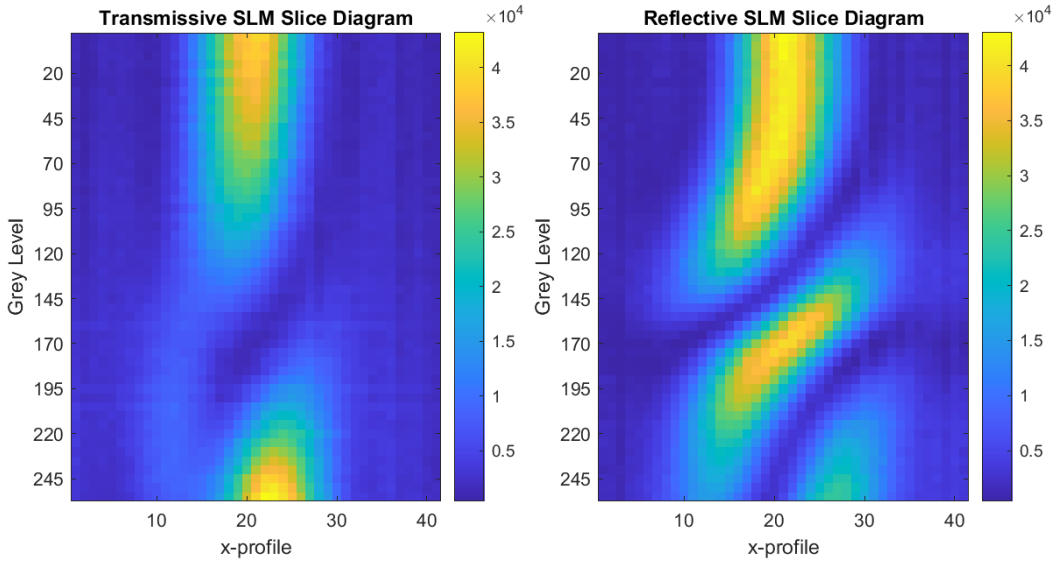

(a) Transmissive SLM (b) Reflective SLM

Figure 12: Slice diagrams from the transmissive and reflective SLMs. Each row represents a slice taken across the centre of each PSF image along the x-axis. The grey levels increase from top to bottom, in steps of 5.

In the Slice Diagrams it is clear to see how the PSF splits into two, and in the case of the TSLM, becomes much more faint. For the RSLM, however, this isn't an issue, with the amplitude splitting equally between the two peaks in the PSF. While this shows that both SLM's are capable of producing this discontinuity, the amplitude modulation from the TSLM is an issue.

In Figure 13, the ratio of the peaks is shown, which have been calculated using Equation 3. One could use such a graph to determine the phase difference between two adjoining segments on, for example, a segmented mirror.

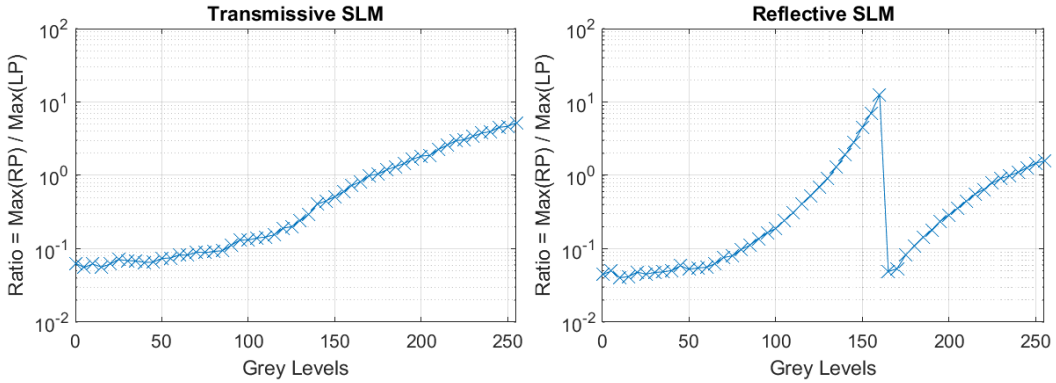

(a) (b)

Figure 13: Peak Ratio comparison of the right and left peaks from the split PSF images (Figure 10).

4. DISCONTINUITY PROFILES

Additionally, we used a FISBA interferometer to examine the transition zone for phase discontinuities. Here, for both SLMs, we look at four different phase steps, which are then normalised and compared to determine the width of the transition zone. Figure 14 shows the results for the transmissive SLM, and Figure 15 for the reflective.

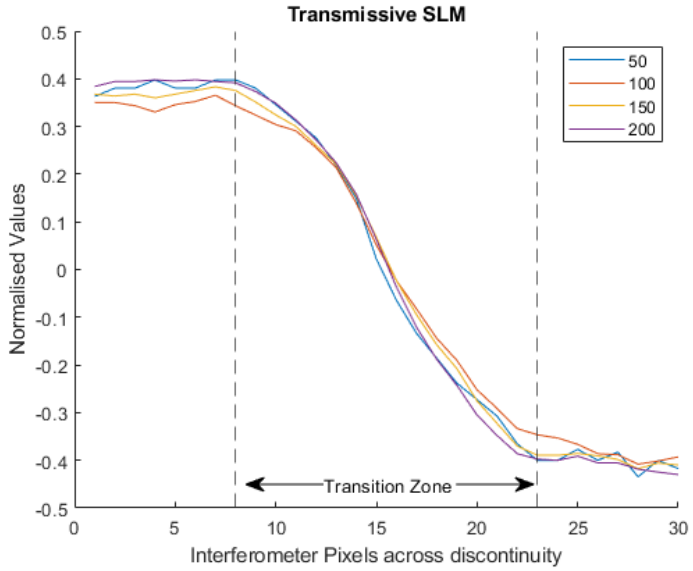

Figure 14: Transition zone across the transmissive SLM. The width of the discontinuity is approximately 15 pixels for all grey level value differences.

From Figure 14 and 15, one might immediately determine that the reflective SLM produces sharper discontinuities than the transmissive one. However, the pixel sizes for the two SLMs differ. Considering the size of pixels on the interferometer of 10 μm, the TSLM and RSLM produce discontinuities over 150 μm and 100 μm respectively. However, on the SLMs, this corresponds to 4.16 and 6.6 pixels respectively. This means that although the RSLM produces sharper discontinuities, it requires more pixels to do so.

5. FUTURE WORK

The SAWS technique proposed by Deo [1] for application to 8-m telescopes could also be applied to ELTs. Figure 16 shows a suitable Golay-type mask [2], which provides an evenly spaced, hexagonal autocorrelation pattern.

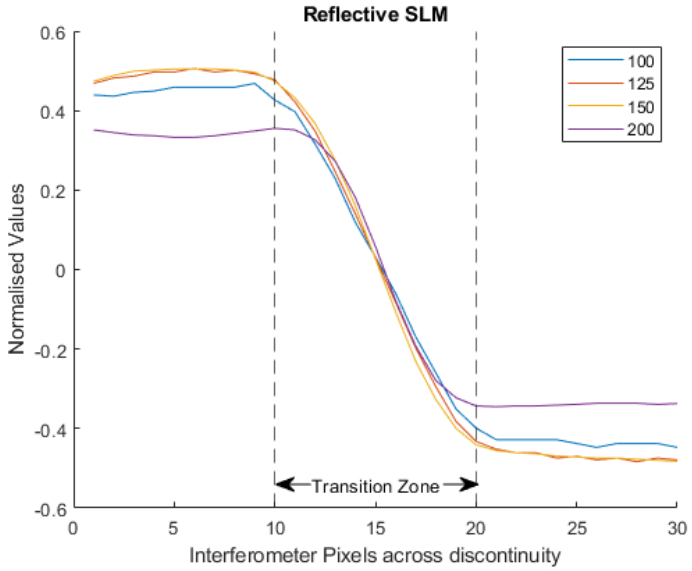

Figure 15: Transition zone across the reflective SLM. The width of the discontinuity is approximately 10 pixels for all grey level value differences.

Table 2: Comparison of the width of the transition zones for the transmissive and reflective SLMs. the transition zone. The values in brackets refer to the integer number of pixels on the device across the transition. Interferometer pixel diameter is $10\mu m$.

	Pixel Diameter	**Transition Zone Width**		
	(μm)	(Interferometer Pixels)	(SLM Pixels)	(μm)
TSLM	36	15	4.16 (5)	150
RSLM	15	10	6.6 (7)	100

The effects of residual tip-tilt and higher-order wavefront errors would need to be evaluated, and this could be carried out using either transmissive or reflective SLMs.

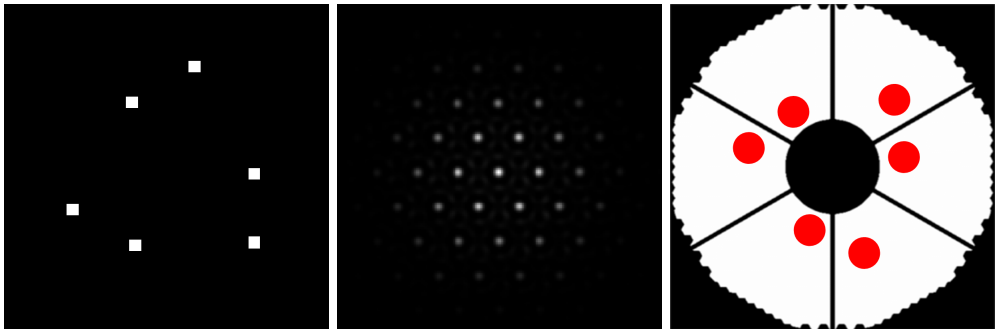

(a) (b) (c)

Figure 16

The PRC method could also be used to detect differential piston between mirror segments, but may not be useful for the detection of piston errors between ELT petals if the spider with is larger than the value of r_0 at the sensing wavelength. The subaperture images would then be seeing-limited and the binary structure due to piston errors would be lost.

6. CONCLUSION

Here, we have presented a comparison of a reflective and a transmissive SLM when used to generate discontinuous phases. We have used the sparse aperture wavefront sensing (SAWFS) method to determine the phase difference between two areas of the transmissive SLM, and used peak ratio comparison (PRC) to compare the ability of the two devices to generate phase discontinuities.

By using SAWFS, we can clearly see that an input phase difference is retrievable in a lab-based system. Deviations from the expected linear response can be attributed to a non-optimal grey level to phase change calibration for the TSLM. The 4-hole mask data produced the best result, clearly showing the phase difference measured from the auto-correlation spots corresponding to pairs of apertures for which a phase difference is input, and none for those that do not experience a phase difference.

Using PRC, it is clear to see the effect the amplitude modulation of the twisted nematic liquid crystals on the transmissive device has, reducing the light throughput and resulting in much noisier results for a phase difference of π (Grey level of 170, Figure 10a). From these measurements, we can also see that the TSLM does not produce a full wave of phase change over 255 grey levels. This confirms the manufacturer's specifications in Table 1 which gives a phase modulation of only 1.8π for this device. The RSLM was able to produce a larger phase change, with a constant amplitude throughout the range of grey levels. This shows that for this method, using non-twisted nematic liquid crystals, such as the parallel-aligned LCs in the RSLM, would be the best option.

To use either SAWFS or PRC on a telescope such as the ELT, the effects of residual tip, tilt, and turbulence on these results would need to be investigated, as well as the width of the spiders for the PRC method between ELT petals. In order to investigate this in the lab, one must make a careful consideration of the type of SLM to use. A transmissive SLM may be easier to implement into an established bench set-up, but can only operate in a phase-mostly configuration with a reduced range of phase modulation. The reflective SLM, however, can provide phase-only modulation, and over a greater range, with the downside of needing additional reflections in the system. Regardless of the device, SLMs provide an excellent way of investigating the effects of petal modes on telescopes, and well as providing an easily reconfigurable and relatively affordable way to test the methods used to measure these discontinuities.

References

[1] Vincent Deo et al. "Controlling petals using fringes: discontinuous wavefront sensing through sparse aperture interferometry at Subaru/SCExAO". In: *Adaptive Optics Systems VIII*. Vol. 12185. SPIE. 2022, pp. 285–297.

[2] Marcel JE Golay. "Point arrays having compact, nonredundant autocorrelations". In: *JOSA* 61.2 (1971), pp. 272–273.

[3] Julien Milli et al. "Low wind effect on VLT/SPHERE: impact, mitigation strategy, and results". In: *Adaptive Optics Systems VI*. Vol. 10703. SPIE. 2018, pp. 752–771.

[4] Jean-François Sauvage et al. "Low Wind Effect, the main limitation of the SPHERE instrument". In: *Adaptive Optics for Extremely Large Telescopes 4–Conference Proceedings*. Vol. 1. 1. 2015.

[5] Jean-François Sauvage et al. "Tackling down the low wind effect on SPHERE instrument". In: *Adaptive Optics Systems V*. Vol. 9909. SPIE. 2016, pp. 408–416.

[6] Achim Schumacher, Nicholas Devaney, and Luzma Montoya. "Phasing segmented mirrors: a modification of the Keck narrow-band technique and its application to extremely large telescopes". In: *Applied Optics* 41.7 (2002), pp. 1297–1307.

[7] Michael J Wilby et al. "Laboratory verification of Fast & Furious phase diversity: Towards controlling the low wind effect in the SPHERE instrument". In: *Astronomy & Astrophysics* 615 (2018), A34.